

Nuclear Structure Effects on Hyperfine Splittings in Ordinary and Muonic Deuterium

Chen Ji,^{1,2,*} Xiang Zhang,¹ and Lucas Platter^{3,4}

¹Key Laboratory of Quark and Lepton Physics, Institute of Particle Physics,
Central China Normal University, Wuhan 430079, China

²Southern Center for Nuclear-Science Theory, Institute of Modern Physics,
Chinese Academy of Sciences, Huizhou 516000, China

³Department of Physics and Astronomy, University of Tennessee, Knoxville, TN 37996, USA

⁴Physics Division, Oak Ridge National Laboratory, Oak Ridge, TN 37831, USA

(Dated: November 23, 2023)

Precision spectroscopy of hyperfine splitting (HFS) is a crucial tool for investigating the structure of nuclei and testing quantum electrodynamics (QED). However, accurate theoretical predictions are hindered by two-photon exchange (TPE) effects. We propose a novel formalism that accounts for nuclear excitations and recoil in TPE, providing a model-independent description of TPE effects on HFS in light ordinary and muonic atoms. Combining our formalism with pionless effective field theory at next-to-next-to-leading order, the predicted TPE effects on HFS are 41.2(2.6) kHz and 0.116(9) meV for the 1S state in deuterium and the 2S state in muonic deuterium. These results are within 1.4-1.7 σ from recent measurements and highlight the importance of nuclear structure effects on HFS and indicate the value of more precise measurements in future experiments.

Introduction. Precision laser spectroscopy of atomic transitions informs on the structure of nuclei and tests the accuracy of bound-state quantum electrodynamics (QED). Measurements of Lamb shifts in light, muonic atoms have provided nuclear charge radii at unprecedented accuracy [1–5]. In these experiments, a solid understanding of nuclear structure effects is crucial [6–10].

High-precision spectroscopy measurements of hyperfine splitting (HFS) have provided valuable insights into the nuclear magnetic structure. These measurements have been conducted on light atoms such as ^1H , ^3He , and $^6,7\text{Li}$ [11–15], as well as their muonic counterparts including $\mu^{1,2}\text{H}$ and $\mu^3\text{He}^+$ [2–4]. HFS, predominantly governed by the short-range interaction between the nuclear and lepton magnetic moments [16–18], offers an ideal probe for studying the elastic and inelastic structure of nucleons and nuclei.

Accurate theoretical predictions for HFS in both ordinary and muonic atoms are limited by nuclear structure effects, entering through two-photon exchange (TPE). The elastic TPE, encoded in the *Zemach radius* r_Z , arises from the convolution of the nuclear charge and magnetic densities [19, 20]. The inelastic TPE, namely the nuclear polarizability, stems from nuclear virtual excitations.

For ^2H and $\mu^2\text{H}$, the discrepancy between the measured HFS and the calculated QED contribution for the 1S state of ^2H is [12, 18].

$$\nu_{\text{exp}}(^2\text{H}) - \nu_{\text{QED}}(^2\text{H}) = 45.2 \text{ kHz}, \quad (1)$$

and for the 2S state of $\mu^2\text{H}$ is [21, 22]

$$\nu_{\text{exp}}(\mu^2\text{H}) - \nu_{\text{QED}}(\mu^2\text{H}) = 0.0966(73) \text{ meV}. \quad (2)$$

These discrepancies mainly arise from TPE. However, an accurate, uncertainty-quantified, and model-independent

prediction of the TPE effect on HFS has not been achieved yet [22–27]. For instance, the conventional Low-term formalism inadequately accounts for nuclear excitations, thus providing an incomplete description [24, 25].

This paper introduces a new formalism for the TPE effect on HFS, that accurately incorporates nuclear excitations and recoil. Using pionless effective field theory (π EFT) at next-to-next-to-leading order (NNLO), we then evaluate TPE contributions in ^2H and $\mu^2\text{H}$. The formalism offers a model-independent description of the TPE effect with systematic uncertainty quantification, showing consistency with $\nu_{\text{exp}} - \nu_{\text{QED}}$ in ^2H and $\mu^2\text{H}$.

Two-Photon Exchange Theory. HFS of $ns_{1/2}$ states is dominated by contact interactions between the lepton spin $\sigma_\ell/2$ and the nuclear spin \mathbf{I} [16–18]

$$\mathcal{H}_I = \frac{2\pi\alpha g_m}{3m_\ell m_N} \phi_n^2(0) \boldsymbol{\sigma}^{(\ell)} \cdot \mathbf{I}, \quad (3)$$

where α is the electromagnetic fine structure constant, g_m denotes the nuclear magnetic g-factor, and m_ℓ (m_N) is the lepton (nucleon) mass. $\phi_n^2(0) = (Z\alpha)^3 m_R^3 / (n^3\pi)$ is the wave function squared of the atomic $ns_{1/2}$ state at the origin, with m_R denoting the lepton-nucleus reduced mass. Its contribution to HFS is at α^4 and is evaluated as the expectation on the atomic hyperfine state by

$$E_F = \langle (ns_{1/2}, N_0 I) F M_F | \mathcal{H}_I | (ns_{1/2}, N_0 I) F M_F \rangle, \quad (4)$$

where $|N_0 I\rangle$ is the nuclear ground state with spin I , and F and M_F denote the total angular momentum and its z-projection.

The TPE effect arises at α^5 , driven by doubly virtual photon exchanges between the nucleus and the lepton, as illustrated in Fig. 1. The corresponding operator is



FIG. 1. Doubly virtual two-photon exchange diagrams.

expressed in Lorenz gauge as [25]

$$\mathcal{H}_{2\gamma} = i(4\pi\alpha)^2 \phi_n^2(0) \int \frac{d^4q}{(2\pi)^4} \frac{\eta_{\mu\nu}(q) T^{\mu\nu}(q, -q)}{(q^2 + i\epsilon)^2 (q^2 - 2m_\ell q_0 + i\epsilon)}, \quad (5)$$

where η and T respectively represent the lepton and nuclear tensors. Only the lepton-spin dependent part $\tilde{\eta}^{\mu\nu} = iq_0 \epsilon^{0\mu\nu i} \sigma_i^{(\ell)} + i\epsilon^{\mu\nu ij} \sigma_i^{(\ell)} q_j$ of the lepton tensor contributes to HFS. The third diagram in Fig. 1 is the nuclear seagull tensor $B_{\mu\nu}$. The charge-current part B_{0m} is of relativistic order at $1/m_N^2$. The current-current part B_{ij} gets canceled due to crossing symmetry [25, 28].

TPE polarizability. We find the inelastic TPE operators by using the spin-dependent part of the lepton tensor and incorporating a summation over nuclear excitations in the nuclear tensor [25]

$$\mathcal{H}_{\text{pol}}^{(0)} = \frac{i\alpha^2 \phi_n^2(0)}{2\pi m_\ell^2} \int d\omega \int \frac{d^3q}{q^4} h^{(0)}(\omega, |\mathbf{q}|) \boldsymbol{\sigma}^{(\ell)} \cdot \{ \mathbf{q} \times \mathbf{J}(-\mathbf{q}), J_0(\mathbf{q}) \} \delta(\omega - \omega_N), \quad (6)$$

$$\mathcal{H}_{\text{pol}}^{(1)} = \frac{i\alpha^2 \phi_n^2(0)}{2\pi m_\ell^2} \int d\omega \int \frac{d^3q}{q^2} h^{(1)}(\omega, |\mathbf{q}|) \boldsymbol{\sigma}^{(\ell)} \cdot [\mathbf{J}(-\mathbf{q}) \times \mathbf{J}(\mathbf{q})] \delta(\omega - \omega_N), \quad (7)$$

where ω_N denotes the excitation energy of the nuclear state. $\mathcal{H}_{2\gamma}^{(0)}$ involves the charge-current transition matrix with the two operators in anti-commutation. $\mathcal{H}_{2\gamma}^{(1)}$ involves the current-current matrix with the two currents in commutation, and is one order higher in $1/m_N$. The kernels $h^{(0,1)}$ are

$$h^{(0)}(\omega, q) = \left[2 + \frac{\omega}{E_q} \right] \frac{E_q^2 + m_\ell^2 + E_q \omega}{(E_q + \omega)^2 - m_\ell^2} - \frac{2q + \omega}{q + \omega}, \quad (8)$$

$$h^{(1)}(\omega, q) = \frac{1}{E_q} \frac{E_q^2 + m_\ell^2 + E_q \omega}{(E_q + \omega)^2 - m_\ell^2} - \frac{1}{q + \omega}, \quad (9)$$

with $E_q = \sqrt{q^2 + m_\ell^2}$.

To obtain the polarizability corrections $E_{\text{pol}}^{(0,1)}$, we replace \mathcal{H}_1 with $\mathcal{H}_{\text{pol}}^{(0,1)}$ in Eq. (4). Using the Wigner-Eckart theorem, we factorize the lepton and nuclear matrix elements in $E_{\text{pol}}^{(0,1)}$, expressing them as ratios to E_F . We write J_0 as charge density ρ and decompose \mathbf{J} into convection (\mathbf{J}_c) and magnetic (\mathbf{J}_m) currents. This leads to

photo-induced nuclear sum rules:

$$E_{\text{pol}}^{(0)} = \frac{6\alpha m_N E_F}{\pi m_l g_m I} \int_{\omega_{\text{th}}}^{\infty} d\omega \int_0^{\infty} dq h^{(0)}(\omega, q) S^{(0)}(\omega, q), \quad (10)$$

$$E_{\text{pol}}^{(1)} = - \frac{6\alpha m_N E_F}{\pi m_l g_m I} \int_{\omega_{\text{th}}}^{\infty} d\omega \int_0^{\infty} dq h^{(1)}(\omega, q) S^{(1)}(\omega, q), \quad (11)$$

where $\omega_{\text{th}} = (\gamma^2 + q^2/4)/m_N$ is the minimum deuteron excitation energy in the inelastic TPE. The nuclear excitations in the deuteron are represented by the scattering state $|\psi_{\mathbf{p}}\rangle$. The deuteron charge-magnetic ($S^{(0)}$) and convection-magnetic ($S^{(1)}$) response functions are

$$S^{(0)}(\omega, q) = \frac{m_N p}{64\pi^4 q^2} \iint d\hat{p} d\hat{q} \text{Im}(\langle N_0 II | \rho(-\mathbf{q}) | \psi_{\mathbf{p}} \rangle \langle \psi_{\mathbf{p}} | [\mathbf{q} \times \mathbf{J}_m(\mathbf{q})]_3 | N_0 II \rangle) \quad (12)$$

$$S^{(1)}(\omega, q) = \frac{m_N p}{64\pi^4} \iint d\hat{p} d\hat{q} \epsilon^{3jk} \times \text{Im}(\langle N_0 II | \mathbf{J}_{c,j}(-\mathbf{q}) | \psi_{\mathbf{p}} \rangle \langle \psi_{\mathbf{p}} | \mathbf{J}_{m,k}(\mathbf{q}) | N_0 II \rangle), \quad (13)$$

where $|N_0 II\rangle$ denotes the nuclear ground state with spin maximally projected in the z-direction. For the deuteron, its nuclear excitation involves the two-nucleon scattering states at relative momentum $p = \sqrt{m_N \omega - \gamma^2 - q^2/4}$.

Elastic TPE. The elastic TPE contribution involves the insertion of the momentum-boosted nuclear ground state into the nuclear tensor $T_{\mu\nu}$, leading to

$$E_{\text{el}}^{(0)} = \frac{2\alpha E_F}{\pi m_l} \int_0^{\infty} dq \left[h^{(0)}\left(\frac{q^2}{4m_N}, q\right) F_{md}(q) F_{ed}(q) - \frac{4m_l m_R}{q^2} \right], \quad (14)$$

$$E_{\text{el}}^{(1)} = - \frac{\alpha E_F}{2\pi m_l m_N} \int_0^{\infty} dq q^2 h^{(1)}\left(\frac{q^2}{4m_N}, q\right) F_{md}(q) F_{ed}(q), \quad (15)$$

where $q^2/(4m_N)$ is the deuteron recoil energy in the elastic TPE process. The deuteron electric and magnetic form factors, F_{ed} and F_{md} are normalized to 1 at $q = 0$. The function $h^{(0)}$ is approximated by $4m_l m_R/q^2$ when taking $m_N \gg m_l$, changing $E_{\text{el}}^{(0)}$ to the pure Zemach contribution $E_{\text{zem}} = -2\alpha m_R r_Z$ [19, 20]. The subtraction term in Eq. (14) cancels the infrared divergence of the q -integration and prevents a double counting in the iteration of the lowest-order single-photon exchange in the point-nucleus limit [29]. $E_{\text{el}}^{(1)}$ is also a convolution of nuclear magnetic and electric densities but is suppressed by $1/m_N$ relative to $E_{\text{el}}^{(0)}$.

A higher-order correction to $E_{\text{el}}^{(0)}$ arises from the deuteron S-to-D-state mixing, and is given by

$$E_{\text{el-sd}}^{(0)} = \frac{\alpha \mu_Q E_F}{3\pi m_l} \int_0^{\infty} dq q^2 h^{(0)}\left(\frac{q^2}{4m_N}, q\right) F_{md}(q) F_{Qd}(q), \quad (16)$$

where F_{Qd} denotes the deuteron quadrupole form factor, which is normalized to 1 at $q = 0$.

Single-nucleon TPE. An additional correction to HFS arises from TPE between the lepton and a single nucleon, and includes the nucleon's Zemach, recoil, and polarizability effects. When embedded in a nucleus, the single-nucleon TPE contributions in ${}^2\text{H}$ and $\mu^2\text{H}$ are [22]

$$E_{1N} = -\frac{2\alpha m_l E_F}{g_m(m_l + m_p)} (\kappa_p \tilde{r}_Z^p + \kappa_n \tilde{r}_Z^n). \quad (17)$$

where \tilde{r}_Z^p and \tilde{r}_Z^n represent the effective proton and neutron Zemach radii, accounting for the full single-nucleon TPE effects [30–34].

Pionless effective field theory. We employ the identical Lagrangian used in Ref. [35] to compute the two-nucleon bound and scattering states utilizing dimensional regularization and power-divergence subtraction (PDS) renormalization. In addition, we include the NNLO S-to-D-wave mixing operator [36–38]

$$\mathcal{L}_{sd} = \frac{C_0^{(sd)}}{4} d_i^\dagger \left[N^T P^j (\overleftrightarrow{\nabla}_i \overleftrightarrow{\nabla}_j - \frac{\delta_{ij}}{3} \overleftrightarrow{\nabla}^2) N \right] + \text{h.c.}, \quad (18)$$

where $\overleftrightarrow{\nabla} \equiv \overleftarrow{\nabla} - \overrightarrow{\nabla}$, γ denotes the deuteron binding momentum and μ the PDS renormalization scale. $C_0^{(sd)} = -6\sqrt{2}\pi\eta_{sd}/[m_N\gamma^2(\mu-\gamma)]$ [36–38] matches the deuteron's asymptotic D-to-S wave ratio $\eta_{sd} = 0.0252$ [39].

P-wave contact interactions enter $\mathcal{N}^3\text{EFT}$ at N^3LO [40, 41]. Furthermore, the relativistic correction to the kinetic term is suppressed by $1/m_N^2$ [42], thus of N^4LO size. We neglect these higher-order contributions in this work.

The one-nucleon current originates from minimal substitution in the free part of the Lagrangian and is [40, 42].

$$\begin{aligned} \mathcal{L}_{\text{EM},1b} = & -\frac{e}{2} N^\dagger [F_{es}(q) + \tau_3 F_{ev}(q)] N A_0 \\ & - \frac{ie}{4m_N} N^\dagger \overleftrightarrow{\nabla} [F_{es}(q) + \tau_3 F_{ev}(q)] N \cdot \mathbf{A} \\ & + \frac{e}{2m_N} N^\dagger [\kappa_0 F_{ms}(q) + \kappa_1 \tau_3 F_{mv}(q)] \boldsymbol{\sigma} \cdot \mathbf{B} N, \quad (19) \end{aligned}$$

where $\boldsymbol{\sigma}$ denotes the nucleon Pauli matrix vector. The nucleon isoscalar and isovector anomalous magnetic factors denoted as κ_0 and κ_1 , are related to the magnetic factors of the proton and neutron by $\kappa_0 = (\kappa_p + \kappa_n)/2$ and $\kappa_1 = (\kappa_p - \kappa_n)/2$. For the nucleon electric and magnetic isoscalar and isovector form factors, we use the recent parametrization based on dispersion analysis of the time- and space-like eN scattering data [43–45].

Two-nucleon currents appear at higher orders in $\mathcal{N}^3\text{EFT}$. Introducing covariant derivatives in the np spin-triplet interaction gives rise to a two-nucleon convection current at NLO, whose interaction Lagrangian is

$$\mathcal{L}_{2,C} = \frac{ieC_2}{4} F_{ev}(q) d_i^\dagger (N^T \overleftrightarrow{\nabla} P_i \tau_3 N) \cdot \mathbf{A} + \text{h.c.}, \quad (20)$$

where C_2 represents the known coefficient of the two-nucleon NLO interaction [42]. $\mathcal{L}_{2,C}$ does not contribute to nuclear electric form factors but affects nuclear polarization. Furthermore, the two-nucleon magnetic current, which couples with the np spin-triplet interaction, emerges at NLO but not through minimal substitution:

$$\mathcal{L}_{2,B} = -ieL_2 F_{ms}(q) \epsilon_{ijk} d_i^\dagger d_j B_k + \text{h.c.}, \quad (21)$$

with $L_2 = (g_m - 2\kappa_0)\pi/[2m_N\gamma(\mu-\gamma)^2]$ determined by matching to the measured magnetic g-factor. The two-nucleon magnetic current causes the np spin-singlet-to-triplet transition to emerge at NLO but does not contribute to TPE in HFS due to spin-parity selection rules. Other two-nucleon currents are beyond NNLO [40, 42].

The transition matrices necessary for calculating the response functions in Eqs. (12,13) are determined using a similar approach as in Ref. [35]. The detailed expressions can be found in the supplementary material [46].

Results. The TPE correction to HFS consists of the elastic, polarizability, and single-nucleon contributions

$$E_{\text{TPE}}^{\text{HFS}} = E_{\text{el}} + E_{\text{pol}} + E_{1p} + E_{1n}. \quad (22)$$

The response functions in Eqs. (12, 13) are numerically evaluated in the $\mathcal{N}^3\text{EFT}$ framework. The regulator independent results indicate the model independence of the prediction. Fig. 2 displays the charge-magnetic response function $S^{(0)}$, S-D mixing correction $S_{\text{sd}}^{(0)}$, and the convection-magnetic one $S^{(1)}$, as functions of the excitation energy ω at a fixed transfer momentum $q = 50$ MeV. $S^{(0)}$, which dominates in the polarizability effect, is calculated at NNLO, while $S^{(1)}$, whose contribution is suppressed by $1/m_N$, is evaluated at NLO. Following Ref. [35, 47, 48], $S^{(0,1)}$ are Z_d -improved for better accuracy by accounting for the remaining effective range correction in the deuteron asymptotic normalization constant. A relative uncertainty of 3.5% (11%) is assigned to $S^{(0)}$ ($S^{(1)}$), due to omitted N^3LO (NNLO) corrections. $S_{\text{sd}}^{(0)}$, expected to enter at NNLO, carries a relative uncertainty of 33% due to its omitted higher-order correction. Inserting the response functions in Eqs. (10,11) leads to the polarizability effects $E_{\text{pol}} = E_{\text{pol}}^{(0)} + E_{\text{pol}}^{(1)} + E_{\text{pol,sd}}^{(0)}$.

With the deuteron form factors evaluated in $\mathcal{N}^3\text{EFT}$, the elastic TPE is a summation of contributions in Eqs. (14–16), $E_{\text{el}} = E_{\text{el}}^{(0)} + E_{\text{el}}^{(1)} + E_{\text{el,sd}}^{(0)}$. It is different from the Zemach contribution E_{zem} due to the additional recoil corrections in E_{el} . The prediction of r_Z from $\mathcal{N}^3\text{EFT}$ is mainly determined by the deuteron S wave, with a 3.2% correction due to S-D mixing:

$$r_{Z,\text{th}}^D = 2.691 \text{ fm} - 0.086 \text{ fm} = 2.605(91) \text{ fm}, \quad (23)$$

with a 3.5% uncertainty from the N^3LO correction. The result is consistent with the calculation using the chiral EFT potential [49], and agrees with the experimental value $r_{Z,\text{exp}} = 2.593(16) \text{ fm}$ within 1σ .

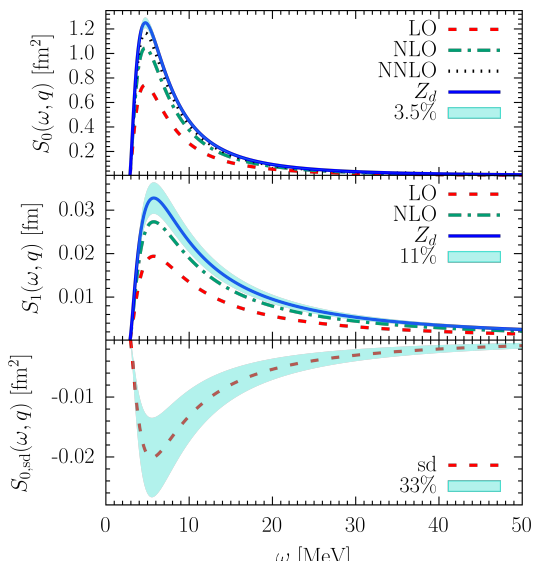


FIG. 2. The response functions $S^{(0)}$ (top panel), $S^{(1)}$ (middle panel), and $S_{sd}^{(0)}$ (bottom panel) are shown as functions of ω for a fixed $q = 50$ MeV. The leading, sub-leading, sub-sub-leading, and Z_d -improved results are represented by the red dashed, green dot-dashed, black dotted, and blue solid lines, respectively (color online). The light-blue band represents the uncertainty error from omitted higher-order corrections.

The single-nucleon TPE contributions from Eq. (17) need inputs for $\tilde{r}_Z^{p,n}$, which accounts for the Zemach, recoil, and polarizability effects from proton and neutron. The proton TPE contributions to HFS in H and μH were determined with high accuracy by using constraints from HFS spectroscopy measurements [32, 50], while the neutron TPE effects were determined using a dispersive calculation [30, 31]. These nucleon TPE effects are transformed into $\tilde{r}_Z^{p,n}$ for ordinary and muonic atoms using a scaling approach [22]:

$$\begin{aligned} \tilde{r}_Z^{p,e} &= 0.883(2) \text{ fm}, & \tilde{r}_Z^{p,\mu} &= 0.906(2) \text{ fm}, \\ \tilde{r}_Z^{n,e} &= 0.347(38) \text{ fm}, & \tilde{r}_Z^{n,\mu} &= 0.102(39) \text{ fm}. \end{aligned} \quad (24)$$

Table I summarizes the elastic, polarizability, and single-nucleon TPE contributions to HFS, comparing our predictions with experimental values and theoretical results from previous studies. E_{el} and E_{pol} are consistently calculated in the $\mathcal{N}^3\text{EFT}$ at the same order and are strongly anti-correlated. Therefore, we assign a 3.5% uncertainty to the combination of $E_{el} + E_{pol}$, reflecting the N^3LO correction. This uncertainty is square summed with the one from the single-nucleon contributions to estimate the total TPE uncertainty. In the ${}^2\text{H}$ 1S state, the prediction for E_{TPE} is 41.7(2.6) kHz, which deviates from $\nu_{\text{exp}} - \nu_{\text{qed}}$ (1) by 7% and falls within 1.3σ of the combined theory-experiment uncertainty. For the $\mu^2\text{H}$ 2S state, the predicted E_{TPE} is 0.118(9) meV, differing from $\nu_{\text{exp}} - \nu_{\text{qed}}$ (2) by 17%, within 1.7σ . E_{TPE} is insensitive

to the choice of nucleon form factors. With a different parameterization [51] that suggests a larger proton radius, the predicted E_{TPE} changes by only sub-percent.

	${}^2\text{H}$ (1S)	$\mu^2\text{H}$ (1S)	$\mu^2\text{H}$ (2S)
$E_{el}^{(0)}$	-41.2	-1.004	-0.126
$E_{el}^{(1)}$	-1.95	-0.011	-0.0014
$E_{el,sd}^{(0)}$	0.97	0.030	0.0037
$E_{pol}^{(0)}$	122.2	3.109	0.389
$E_{pol}^{(1)}$	-7.8	-0.129	-0.016
$E_{pol,sd}^{(0)}$	-4.5	-0.116	-0.014
E_{1p} [32]	-35.54(8)	-1.018(2)	-0.1272(2)
E_{1n} [30]	9.6(1.0)	0.08(3)	0.010(4)
E_{el}	-41.9(1.5)	-0.985(34)	-0.123(4)
E_{pol}	109.8(3.8)	2.86(10)	0.358(13)
E_{TPE}	41.7(2.6)	0.940(73)	0.118(9)
Ref. [26, 27]	43		
Ref. [24, 25] _{mod}	64.5		
Ref. [22]		0.304(68)	0.0383(86)
$\nu_{\text{exp}} - \nu_{\text{qed}}$ [18, 21]	45		0.0966(73)

TABLE I. Single-nucleon, nuclear elastic and polarizability contributions to TPE. The subscript ‘mod’ denotes modifications made to the findings in Ref. [24, 25], incorporating nucleon recoil and polarizability effects.

In comparison, the TPE effect on HFS in ${}^2\text{H}$ was initially calculated using the zero-range approximation [26, 27], showing agreement within 5% with $\nu_{\text{exp}} - \nu_{\text{qed}}$ (1). This formalism was revisited in Ref. [23] to include higher-order elastic recoil corrections and was extended to estimate polarizability effects on HFS in $\mu^2\text{H}$ [21]. This approach introduces a 33% discrepancy in the deuteron’s asymptotic behavior and an unquantified model-dependent uncertainty through an arbitrary energy-integration cutoff. Thus, their agreement with experiments may be accidental.

Alternatively, the Low-term formalism takes the heavy-nucleon-mass limit and evaluates $E_{el} + E_{pol}$ using the closure approximation without explicitly treating nuclear excitations. However, the approximation becomes inaccurate when the momentum scale of nuclear excitations is comparable to m_l or γ , changing the infrared q -dependence in Eq. (5). Their predicted TPE effect in ${}^2\text{H}$ was 46 kHz, whose agreement with $\nu_{\text{exp}} - \nu_{\text{qed}}$ (1) is accidental due to the omission of single-nucleon recoil and polarizability effects. Adding these corrections, the corresponding modified TPE effects becomes $E_{\text{TPE}}^{\text{HFS}}({}^2\text{H}) = 64$ kHz, disagreeing with $\nu_{\text{exp}} - \nu_{\text{qed}}$ by 43%. The Low-term formalism was extended by including higher-order polarizability corrections to study the TPE effect in $\mu^2\text{H}$ [22], and yielded $E_{\text{TPE}}^{\text{HFS}}(\mu^2\text{H}) = 0.38$ meV, accounting for only 40% of $\nu_{\text{exp}} - \nu_{\text{qed}}$ (2).

Conclusion. The N^3LO corrections in $\mathcal{N}^3\text{EFT}$ limit the accuracy of our prediction for the TPE effect on HFS. As another limiting factor, the uncertainty from the single-

nucleon TPE effect may be much larger than anticipated due to the one-order-of-magnitude discrepancy between the proton polarizability effects to HFS from χ PT [32–34] and from dispersion analysis [30, 31]. This dispute also raises questions about the predicted neutron polarizability. A resolution to the single-nucleon TPE discrepancy requires higher-order χ PT calculations and future HFS measurements of the 1S state in μ H [52–54]. Furthermore, to pin down the single-nucleon effects from HFS in ${}^2\text{H}$ and $\mu^2\text{H}$, it will be crucial to improve the accuracy of calculations of the nuclear-structure part of TPE with $\not\chi$ EFT beyond NNLO or with χ EFT, and to measure HFS in ${}^2\text{H}$ and $\mu^2\text{H}$ with high precision. The formalism developed in this work can also be applied to future investigations of TPE effects on HFS in other light atomic systems.

Acknowledgement. We gratefully acknowledge valuable discussions with Daniel Philips, Sonia Bacca, Thomas Richardson, and Javier Hernandez during the project. CJ extends gratitude to Yong-Hui Lin for sharing the data on nucleon form factors. This work was supported by the National Natural Science Foundation of China (Grant Nos. 12175083, 12335002, and 11805078), the National Science Foundation (Grant No. PHY-2111426), and the Office of Nuclear Physics, US Department of Energy (Contract No. DE-AC05-00OR22725).

* jichen@ccnu.edu.cn

- [1] R. Pohl et al., *Nature* **466**, 213 (2010).
- [2] A. Antognini et al., *Science* **339**, 417 (2013).
- [3] R. Pohl et al., *Science* **353**, 669 (2016).
- [4] K. Schuhmann et al. (CREMA) (2023) [arXiv:2305.11679](https://arxiv.org/abs/2305.11679) [[physics.atom-ph](https://arxiv.org/abs/2305.11679)].
- [5] J. J. Krauth et al., *Nature* **589**, 527 (2021).
- [6] K. Pachucki, *Phys. Rev. Lett.* **106**, 193007 (2011).
- [7] C. Ji, N. Nevo Dinur, S. Bacca, and N. Barnea, *Phys. Rev. Lett.* **111**, 143402 (2013).
- [8] C. Ji, S. Bacca, N. Barnea, O. J. Hernandez, and N. Nevo-Dinur, *J. Phys. G* **45**, 093002 (2018).
- [9] N. Nevo Dinur, C. Ji, S. Bacca, and N. Barnea, *Phys. Lett. B* **755**, 380 (2016).
- [10] O. Hernandez, A. Ekström, N. N. Dinur, C. Ji, S. Bacca, and N. Barnea, *Phys. Lett. B* **778**, 377 (2018).
- [11] H. Hellwig, R. F. C. Vessot, M. W. Levine, P. W. Zitzewitz, D. W. Allan, and D. J. Glaze, *IEEE Trans. Instrum. Meas.* **19**, 200 (1970).
- [12] D. J. Wineland and N. F. Ramsey, *Phys. Rev. A* **5**, 821 (1972).
- [13] S. D. Rosner and F. M. Pipkin, *Phys. Rev. A* **1**, 571 (1970).
- [14] J. Kowalski, R. Neumann, S. Noehte, K. Scheffzek, H. Suhr, and G. z. Putlitz, *Hyperfine Interact.* **15**, 159 (1983).
- [15] H. Guan et al., *Phys. Rev. A* **102**, 030801 (2020).
- [16] C. Schwartz, *Phys. Rev.* **97**, 380 (1955).
- [17] G. K. Woodgate, *Elementary Atomic Structure*, 2nd ed., Oxford science publications (Oxford University Press, London, England, 1983).
- [18] M. I. Eides, H. Grotch, and V. A. Shelyuto, *Phys. Rep.* **342**, 63 (2001).
- [19] A. C. Zemach, *Phys. Rev.* **104**, 1771 (1956).
- [20] J. Friar and I. Sick, *Phys. Lett. B* **579**, 285 (2004).
- [21] J. J. Krauth, M. Diepold, B. Franke, A. Antognini, F. Kottmann, and R. Pohl, *Ann. Phys.* **366**, 168 (2016).
- [22] M. Kalinowski, K. Pachucki, and V. A. Yerokhin, *Phys. Rev. A* **98**, 062513 (2018).
- [23] R. N. Faustov and A. P. Martynenko, *Phys. Rev. A* **67**, 052506 (2003).
- [24] J. L. Friar and G. L. Payne, *Phys. Lett. B* **618**, 68 (2005).
- [25] J. L. Friar and G. L. Payne, *Phys. Rev. C* **72**, 014002 (2005).
- [26] I. B. Khriplovich, A. I. Milshtein, and S. S. Petrosian, *Phys. Lett. B* **366**, 13 (1996).
- [27] I. B. Khriplovich and A. I. Milstein, *J. Exp. Theor. Phys.* **98**, 181 (2004).
- [28] J. Friar and M. Rosen, *Ann. Phys.* **87**, 289 (1974).
- [29] C. E. Carlson, V. Nazaryan, and K. Griffioen, *Phys. Rev. A* **83**, 042509 (2011).
- [30] O. Tomalak, *Eur. Phys. J. A* **55**, 64 (2019).
- [31] O. Tomalak, *Phys. Rev. D* **99**, 056018 (2019).
- [32] A. Antognini, F. Hagelstein, and V. Pascalutsa, *Annu. Rev. Nucl. Part. Sci.* **72**, 389 (2022).
- [33] F. Hagelstein and V. Pascalutsa, *PoS CD15*, 077 (2016).
- [34] F. Hagelstein, *Few Body Syst.* **59**, 93 (2018).
- [35] S. B. Emmons, C. Ji, and L. Platter, *J. Phys. G* **48**, 035101 (2021).
- [36] J.-W. Chen, G. Rupak, and M. J. Savage, *Phys. Lett. B* **464**, 1 (1999).
- [37] X.-D. Ji and Y.-C. Li, *Phys. Lett. B* **591**, 76 (2004).
- [38] S.-i. Ando and C. H. Hyun, *Phys. Rev. C* **72**, 014008 (2005).
- [39] V. G. J. Stoks, R. A. M. Klomp, C. P. F. Terheggen, and J. J. de Swart, *Phys. Rev. C* **49**, 2950 (1994).
- [40] G. Rupak, *Nucl. Phys. A* **678**, 405 (2000).
- [41] J.-W. Chen and M. J. Savage, *Phys. Rev. C* **60**, 065205 (1999).
- [42] J.-W. Chen, G. Rupak, and M. J. Savage, *Nucl. Phys. A* **653**, 386 (1999).
- [43] Y.-H. Lin, H.-W. Hammer, and U.-G. Meißner, *Eur. Phys. J. A* **57**, 255 (2021).
- [44] Y.-H. Lin, H.-W. Hammer, and U.-G. Meißner, *Phys. Lett. B* **816**, 136254 (2021).
- [45] Y.-H. Lin, H.-W. Hammer, and U.-G. Meißner, *Phys. Rev. Lett.* **128**, 052002 (2022).
- [46] See Supplemental Material for the TPE formalism derived in $\not\chi$ EFT.
- [47] D. R. Phillips, G. Rupak, and M. J. Savage, *Phys. Lett. B* **473**, 209 (2000).
- [48] D. R. Phillips and T. D. Cohen, *Nucl. Phys. A* **668**, 45 (2000).
- [49] N. Nevo Dinur, O. J. Hernandez, S. Bacca, N. Barnea, C. Ji, S. Pastore, M. Piarulli, and R. B. Wiringa, *Phys. Rev. C* **99**, 034004 (2019).
- [50] A. Antognini, Y.-H. Lin, and U.-G. Meißner, *Phys. Lett. B* **835**, 137575 (2022).
- [51] J. J. Kelly, *Phys. Rev. C* **70**, 068202 (2004).
- [52] M. Sato et al., *JPS Conf. Proc.* **8**, 025005 (2015).
- [53] C. Pizzolotto et al., *Eur. Phys. J. A* **56**, 185 (2020).
- [54] P. Amaro et al., *SciPost Phys.* **13**, 020 (2022).

Supplemental Material: Nuclear Structure Effects on Hyperfine Splittings in Ordinary and Muonic Deuterium

Chen Ji,^{1,2} Xiang Zhang,¹ and Lucas Platter^{3,4}

¹Key Laboratory of Quark and Lepton Physics, Institute of Particle Physics,
Central China Normal University, Wuhan 430079, China

²Southern Center for Nuclear-Science Theory, Institute of Modern Physics,
Chinese Academy of Sciences, Huizhou 516000, China

³Department of Physics and Astronomy, University of Tennessee, Knoxville, TN 37996, USA

⁴Physics Division, Oak Ridge National Laboratory, Oak Ridge, TN 37831, USA

(Dated: November 23, 2023)

This supplemental material includes a brief review of pionless effective field theory, specifically focusing on the formalism used to compute the two-photon exchange (TPE) process discussed in the main text. We provide a detailed presentation of the Lagrangian formulation for the np system and its connection to both bound and scattering states, and derive the deuteron electromagnetic form factors needed for calculating the elastic TPE. Furthermore, we outline the formulation of the transition matrices and response functions relevant to the inelastic TPE.

PIONLESS EFFECTIVE FIELD THEORY

Lagrangian for the deuteron channel. The pionless effective field theory (π EFT) Lagrangian for the non-relativistic np system in the deuteron channel is composed of the one-body kinetic term and two-nucleon spin-triplet contact interactions [1]

$$\begin{aligned} \mathcal{L} = & N^\dagger \left(i\partial_0 + \frac{\nabla^2}{2m_N} \right) N - C_0 (N^T P_i N)^\dagger (N P_i N) \\ & + \frac{1}{8} C_2 \left[(N^T P_i N)^\dagger (N^T \mathcal{O}_i^{(2)} N) + \text{h.c.} \right] \\ & - \frac{1}{16} C_4 (N^T \mathcal{O}_i^{(2)} N)^\dagger (N^T \mathcal{O}_i^{(2)} N) + \dots, \quad (1) \end{aligned}$$

where $\mathcal{O}_i^{(2)} \equiv \overleftarrow{\nabla}^2 P_i - 2\overleftarrow{\nabla} P_i \overrightarrow{\nabla} + P_i \overrightarrow{\nabla}^2$ is the Galilean invariant operator involving two derivatives. Here, $P_i = \frac{1}{\sqrt{8}} \sigma_2 \sigma_i \tau_2$ represents the np spin-triplet projection operator, where σ_i and τ_i are the spin and isospin Pauli matrices. The operator satisfies $\text{Tr}[P_i^\dagger P_j] = \frac{1}{2} \delta_{ij}$. The values of the low-energy constants (LECs) in Eq. (1) are determined by fitting them to the low-momentum expansion of the np spin-triplet scattering phase shift

$$p \cot \delta_t(p) = -\gamma + \frac{\rho}{2}(p^2 + \gamma^2) + \dots, \quad (2)$$

where the deuteron binding momentum $\gamma = \sqrt{m_N B_d}$ is directly related to the deuteron binding energy of $B_d = 2.2246$ MeV. The effective range for the np spin-triplet state is given by $\rho = 1.764$ fm. The corresponding LECs are expanded as

$$\begin{aligned} C_0 &= C_{0,-1} + C_{0,0} + C_{0,1} + \dots, \\ C_2 &= C_{2,-2} + C_{2,-1} + \dots, \\ C_4 &= C_{4,-3} + \dots. \end{aligned} \quad (3)$$

The use of dimensional regularization and power-divergence subtraction renormalization allows us to express the LECs in terms of the effective range parameters and the renormalization scale μ appearing in Eq. (2). The subscripts in $C_{n,m}$ give the power of momentum n in the operator and m the power of momentum in the coefficient itself [1].

$$\begin{aligned} C_{0,-1} &= -\frac{4\pi}{m_N} \frac{1}{\mu - \gamma}, & C_{0,0} &= \frac{2\pi}{m_N} \frac{\rho\gamma^2}{(\mu - \gamma)^2}, \\ C_{0,1} &= -\frac{\pi}{m_N} \frac{\rho^2\gamma^4}{(\mu - \gamma)^3}, & C_{2,-2} &= \frac{2\pi}{m_N} \frac{\rho}{(\mu - \gamma)^2}, \\ C_{2,-1} &= -\frac{2\pi}{m_N} \frac{\rho^2\gamma^2}{(\mu - \gamma)^3}, & C_{4,-3} &= -\frac{\pi}{m_N} \frac{\rho^2}{(\mu - \gamma)^3}. \end{aligned} \quad (4)$$

The main text of our paper gives additional operators, such as the S-D mixing interaction and one- and two-nucleon currents. These terms will not be repeated here. The np spin-singlet interaction will not be considered as it does not impact the TPE effect on HFS.

np scattering t-matrices. The on-shell triplet-state t-matrix for the np scattering state is expanded at NNLO as follows:

$$\begin{aligned} \mathcal{A}_t(p, p; E) &\approx \left[\mathcal{A}_t^{(0)} + \mathcal{A}_t^{(1)} + \mathcal{A}_t^{(2)} \right] (p, p; E) \\ &= -\frac{4\pi}{m_N} \frac{1}{\gamma + ip} \left[1 + \frac{\rho}{2}(\gamma - ip) + \frac{\rho^2}{4}(\gamma - ip)^2 \right], \quad (5) \end{aligned}$$

where $p = \sqrt{m_N E}$ represents the on-shell momentum, and $\mathcal{A}_t^{(0)}$, $\mathcal{A}_t^{(1)}$, and $\mathcal{A}_t^{(2)}$ give the leading order (LO), next-to-leading order (NLO), and next-to-next-to-leading order (NNLO) contributions to the on-shell scattering amplitude, respectively.

The half-off-shell np spin-triplet scattering t-matrices

at LO, NLO, and NNLO can be obtained using the following expressions [2]:

$$\mathcal{A}_t^{(0)}(k, p; E) = -\frac{4\pi}{m_N} \frac{1}{\gamma + ip}, \quad (6)$$

$$\mathcal{A}_t^{(1)}(k, p; E) = -\frac{2\pi}{m_N} \frac{\rho}{\gamma + ip} \left[\gamma - ip + \frac{k^2 - p^2}{2(\gamma - \mu)} \right], \quad (7)$$

$$\begin{aligned} \mathcal{A}_t^{(2)}(k, p; E) = & -\frac{\pi}{m_N} \frac{\rho^2}{\gamma + ip} [(\gamma - ip)^2 \\ & + \frac{\gamma - ip}{\gamma - \mu} \left(1 + \frac{\gamma + ip}{\gamma - \mu} \right) \frac{k^2 - p^2}{2}], \quad (8) \end{aligned}$$

where k is the off-shell momentum, which appears in the later sections as the momentum of loop integrals.

Deuteron form factors. The deuteron's electric and magnetic form factors are calculated from matrix elements of single-photon operators between deuteron states. The deuteron electric charge form factor at NNLO is given by:

$$\frac{F_{ed}(q)}{F_{es}(q)} = \frac{1}{1 - \gamma\rho} \left[\frac{4\gamma}{q} \arctan \frac{q}{4\gamma} - \gamma\rho \right]. \quad (9)$$

We disregard the relativistic and S-D mixing corrections to the deuteron's electric charge form factor as they only contribute at N⁴LO.

The deuteron's electric quadrupole form factor is generated through the mixing of S- and D-waves in its ground state. The dominant term that contributes to it can be expressed in \mathcal{N} EFT as:

$$\mu_Q \frac{F_{Qd}(q)}{F_{es}(q)} = -\frac{3\sqrt{2}\eta_{sd}}{q^2} \left[1 - \left(1 + \frac{3q^2}{16\gamma^2} \right) \frac{4\gamma}{q} \arctan \frac{q}{4\gamma} \right]. \quad (10)$$

The quadrupole form factor is normalized to $F_{Qd}(0) = 1$, and the LO prediction for the deuteron quadrupole moment is $\mu_Q = \eta_{sd}/(\sqrt{2}\gamma^2) = 0.332 \text{ fm}^2$ [3, 4].

The magnetic form factor F_{md} at NNLO in \mathcal{N} EFT is derived as [1]:

$$\frac{F_{md}(q)}{F_{ms}(q)} = \left[\frac{2\kappa_0/g_m}{1 - \gamma\rho} \left(\frac{4\gamma}{q} \arctan \frac{q}{4\gamma} - 1 \right) + 1 \right], \quad (11)$$

where the inclusion of the two-nucleon magnetic current is crucial for accurately reproducing the measured deuteron magnetic anomalous factor.

TRANSITION MATRICES IN VIRTUAL PHOTON EXCITATION

The deuteron's transition matrix elements from virtual photon excitation are obtained from the Feynman diagrams depicted in Fig. 1. In the \mathcal{N} EFT expansion, contributions to the transition matrices can be classified into

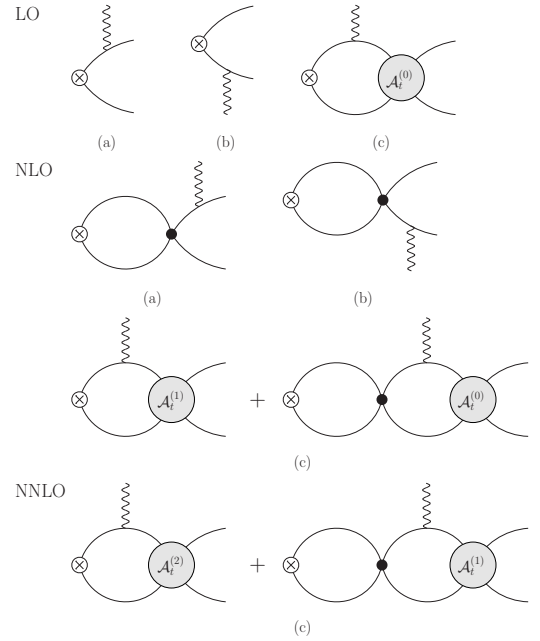


FIG. 1. Deuteron transition matrices at different orders in \mathcal{N} EFT. Group (a) and (b) include diagrams that involve plane-wave excited states with a NN permutation. Group (c) consists of diagrams involving NN final-state interactions.

three groups referred to as (a), (b), and (c). The photon-nucleon vertex encompass the charge-density, convection-current, and magnetic-current operators.

Charge density transition. The transition matrices resulting from the charge density operator can be determined by employing the formulas given in Ref. [2]:

$$\mathcal{T}_a = |Z_d|^{\frac{1}{2}} i\tilde{T}_a N^T(\mathbf{u}) \Pi_+ [F_{es}(q) + \tau_3 F_{ev}(q)] N(\mathbf{v}), \quad (12)$$

$$\mathcal{T}_b = |Z_d|^{\frac{1}{2}} i\tilde{T}_b N^T(\mathbf{u}) [F_{es}(q) + \tau_3 F_{ev}(q)] \Pi_+ N(\mathbf{v}), \quad (13)$$

$$\mathcal{T}_c = 2|Z_d|^{\frac{1}{2}} i\tilde{T}_c F_{es}(q) N^T(\mathbf{u}) \Pi_+ N(\mathbf{v}), \quad (14)$$

where the momenta of the two outgoing nucleon momenta are $\mathbf{u} = -\mathbf{p} + \frac{\mathbf{q}}{2}$ and $\mathbf{v} = \mathbf{p} + \frac{\mathbf{q}}{2}$, and \mathbf{q} is the photon momentum. $Z_d = -8\pi\gamma/[m_N^2(1-\rho\gamma)]$ is the renormalization strength of the deuteron field. We define spin-triplet projection operators with spherical indices that enable to use to carry out calculations for matrix elements with a specific I_z -projection

$$\Pi_{\pm} = i(P_2 \pm iP_1)/\sqrt{2}, \quad \Pi_0 = P_3. \quad (15)$$

These satisfy $\text{Tr} [\Pi_{\alpha} \Pi_{\beta}^{\dagger}] = \frac{1}{2} \delta_{\alpha\beta}$, where α and β take the values $-$, 0 , or $+$.

Summing the transition matrices through NNLO, we

obtain the amplitudes $\tilde{T}_{a,b,c}$:

$$\tilde{T}_a = -\frac{m_N}{\gamma^2 + (\mathbf{p} - \frac{\mathbf{q}}{2})^2} + \frac{m_N \rho}{4(\mu - \gamma)}, \quad (16)$$

$$\tilde{T}_b = -\frac{m_N}{\gamma^2 + (\mathbf{p} + \frac{\mathbf{q}}{2})^2} + \frac{m_N \rho}{4(\mu - \gamma)}, \quad (17)$$

$$\tilde{T}_c = \mathcal{A}_t^{(0)}(E_f) \left[\mathcal{J}_0 + \frac{\rho}{2} \left((\gamma - ip) \mathcal{J}_0 + \frac{m_N^2}{4\pi} \right) \left(1 + \frac{\rho}{2} (\gamma - ip) \right) \right] - \frac{m_N \rho}{4(\mu - \gamma)}, \quad (18)$$

where the loop integral \mathcal{J}_0 is defined in Eq. (48).

Magnetic current transition. By using the one-body magnetic current operator in the photon-nucleon vertices shown in Fig. 1, we obtain the transition matrices induced by the magnetic current:

$$\mathcal{M}_a = \frac{1}{m_N} |Z_d|^{\frac{1}{2}} i \tilde{M}_a N^T(\mathbf{u}) \Pi_+ i(\boldsymbol{\sigma} \times \mathbf{q}) [\kappa_0 F_{ms}(q) + \tau_3 \kappa_1 F_{mv}(q)] N(\mathbf{v}), \quad (19)$$

$$\mathcal{M}_b = \frac{1}{m_N} |Z_d|^{\frac{1}{2}} i \tilde{M}_b N^T(\mathbf{u}) i(\boldsymbol{\sigma}^T \times \mathbf{q}) [\kappa_0 F_{ms}(q) + \tau_3 \kappa_1 F_{mv}(q)] \Pi_+ N(\mathbf{v}), \quad (20)$$

$$\mathcal{M}_c = \frac{4}{m_N} |Z_d|^{\frac{1}{2}} i \tilde{M}_c \text{Tr} [\Pi_+ i(\boldsymbol{\sigma} \times \mathbf{q}) \Pi_+^\dagger] \kappa_0 F_{ms}(q) N^T(\mathbf{u}) \Pi_\alpha N(\mathbf{v}). \quad (21)$$

The two-nucleon current shown in Fig. 2 contributes to the magnetic transition matrices at NNLO. It can be incorporated into the amplitude \tilde{M}_c . By summing up contributions to the magnetic transition through NNLO, we obtain the amplitudes $\tilde{M}_{a,b,c}$ as

$$\tilde{M}_a = \tilde{T}_a; \quad \tilde{M}_b = \tilde{T}_b; \quad \tilde{M}_c = \tilde{T}_c + \frac{m_N (\frac{g_m}{\kappa_0} - 2)}{4\gamma(\gamma + ip)}. \quad (22)$$

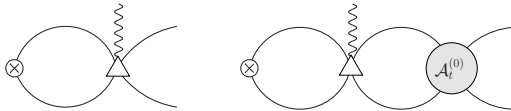


FIG. 2. The deuteron transition matrices with the inclusion of the two-nucleon current, depicted by the upward triangle.

Convection current transition. The transition matrices induced by the convection current can be obtained from the diagrams shown in Fig. 1 with the appropriate single-photon operator used in the calculation. We

obtain

$$\mathcal{C}_a = |Z_d|^{\frac{1}{2}} \frac{\mathbf{p}}{m_N} i \tilde{C}_a N^T(\mathbf{u}) \Pi_+ [F_{es}(q) + \tau_3 F_{ev}(q)] N(\mathbf{v}), \quad (23)$$

$$\mathcal{C}_b = -|Z_d|^{\frac{1}{2}} \frac{\mathbf{p}}{m_N} i \tilde{C}_b N^T(\mathbf{u}) [F_{es}(q) + \tau_3 F_{ev}(q)] \Pi_+ N(\mathbf{v}), \quad (24)$$

$$\mathcal{C}_c = 2|Z_d|^{\frac{1}{2}} \frac{\mathbf{q}}{m_N} i \tilde{C}_c^{(0)} F_{es}(q) N^T(\mathbf{u}) \Pi_+ N(\mathbf{v}). \quad (25)$$

The two-nucleon convection current gives an additional NLO contribution to the transition matrices, as depicted in Fig. 2. Evaluation of the diagram leads to

$$\mathcal{C}_d = |Z_d|^{\frac{1}{2}} \frac{\mathbf{p}}{m_N} i \tilde{C}_d F_{ev}(q) N^T(\mathbf{u}) \Pi_+ \tau_3 N(\mathbf{v}). \quad (26)$$

Since the emergence of the convection current is already suppressed by $1/m_N$ in TPE, we calculate the convection transition matrices up to NLO. This allows us to obtain the corresponding amplitudes, denoted as $\tilde{C}_{a,b,c,d}$:

$$\begin{aligned} \tilde{C}_a &= \tilde{T}_a; \quad \tilde{C}_b = \tilde{T}_b; \quad \tilde{C}_d = -\frac{m_N \rho}{2(\mu - \gamma)}; \\ \tilde{C}_c &= \frac{m_N \omega}{q^2} \mathcal{A}_t^{(0)}(p, p; E_f) \left\{ \mathcal{J}_0 + \frac{m_N}{4\pi \omega} (\gamma + ip) \right. \\ &\quad \left. + \frac{\rho}{2} \left[(\gamma - ip) \mathcal{J}_0 + \frac{m_N^2}{4\pi} \right] \right\}. \end{aligned} \quad (27)$$

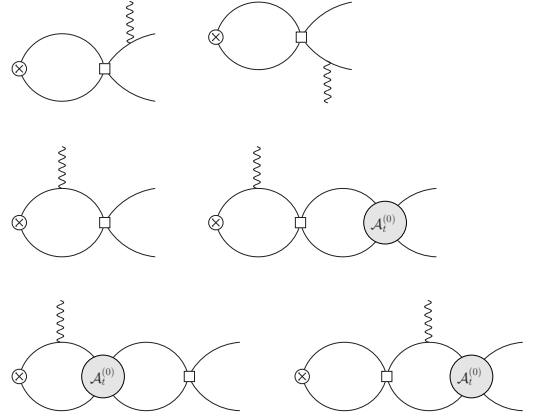


FIG. 3. Deuteron transition matrices incorporating the S-D mixing operator, represented by the square.

S-D mixing in transition. Since the S-D mixing operator emerges at NNLO, we only evaluate its dominant correction to the response function $S^{(0)}$. Its contribution

to the transition matrices, shown in Fig. 3, is as follows:

$$\begin{aligned} \mathcal{Q}_a = & 2|Z_d|^{\frac{1}{2}} i\tilde{Q}_a \text{Tr}[\Pi_+ P_i^\dagger] N^T(\mathbf{u}) P_j \\ & [F_{es}(q) + \tau_3 F_{ev}(q)] N(\mathbf{v})(u_i u_j - \frac{1}{3} u^2 \delta_{ij}), \end{aligned} \quad (28)$$

$$\begin{aligned} \mathcal{Q}_b = & 2|Z_d|^{\frac{1}{2}} i\tilde{Q}_b \text{Tr}[\Pi_+ P_i^\dagger] N^T(\mathbf{u}) \\ & [F_{es}(q) + \tau_3 F_{ev}(q)] P_j N(\mathbf{v})(v_i v_j - \frac{1}{3} v^2 \delta_{ij}), \end{aligned} \quad (29)$$

$$\begin{aligned} \mathcal{Q}_c = & 4|Z_d|^{\frac{1}{2}} i\tilde{Q}_c F_{es}(q) \text{Tr}[\Pi_+ P_i^\dagger] N^T(\mathbf{u}) P_j N(\mathbf{v}) \\ & (q_i q_j - \frac{1}{3} q^2 \delta_{ij}), \end{aligned} \quad (30)$$

$$\begin{aligned} \mathcal{Q}_d = & 4|Z_d|^{\frac{1}{2}} i\tilde{Q}_d F_{es}(q) \text{Tr}[\Pi_+ P_i^\dagger] N^T(\mathbf{u}) P_j N(\mathbf{v}) \\ & (p_i p_j - \frac{1}{3} p^2 \delta_{ij}), \end{aligned} \quad (31)$$

where the amplitudes $\tilde{Q}_{a,b,c,d}$ are given by

$$\begin{aligned} \tilde{Q}_a = & -\frac{3\eta_{sd} m_N}{\sqrt{2}\gamma^2(\gamma^2 + \mathbf{u}^2)}; \quad \tilde{Q}_d = -\frac{6\sqrt{2}\pi\eta_{sd}\mathcal{J}_0}{m_N\gamma^2(\gamma + ip)}; \quad (32) \\ \tilde{Q}_b = & -\frac{3\eta_{sd} m_N}{\sqrt{2}\gamma^2(\gamma^2 + \mathbf{v}^2)}; \quad \tilde{Q}_c = -\frac{6\sqrt{2}\pi\eta_{sd}\bar{J}_Q}{m_N\gamma^2 q^2(\gamma + ip)}. \end{aligned} \quad (33)$$

with \bar{J}_Q defined in Eq. (56).

Response functions. The transition matrices are used in the response functions discussed in the main text. After trace evaluation (see Eqs. (57), (58), and (59)) and integrating over the solid angles of \hat{p} and \hat{q} , we derive the response functions $S^{(0)}$, its S-D mixing correction $S_{sd}^{(0)}$, and $S^{(1)}$ as

$$S^{(0)}(\omega, q) = \frac{p|Z_d|}{12\pi^2} \text{Re} \left[U_{mt,s}^{[0]} \kappa_0 F_{ms} F_{es} + U_{mt,v}^{[0]} \kappa_1 F_{mv} F_{ev} \right], \quad (34)$$

$$\begin{aligned} S^{(1)}(\omega, q) = & \frac{p|Z_d|}{12\pi^2 m_N} \text{Re} \left[(qpU_{mc,s}^{[1]} + q^2 W_{mc,s}^{[0]}) \kappa_0 F_{ms} F_{es} \right. \\ & \left. + qpU_{mc,v}^{[1]} \kappa_1 F_{mv} F_{ev} \right], \end{aligned} \quad (35)$$

$$\begin{aligned} S_{sd}^{(0)}(\omega, q) = & \frac{p|Z_d|}{36\pi^2} \text{Re} \left[\left(\frac{q^2}{4} V_{sd,s}^{[0]} - pqX_{sd,s}^{[1]} + p^2 W_{sd,s}^{[2]} \right) \kappa_0 \right. \\ & \left. F_{es} F_{ms} + \left(\frac{q^2}{4} V_{sd,v}^{[0]} - pqX_{sd,v}^{[1]} + p^2 V_{sd,v}^{[2]} \right) \kappa_1 F_{ev} F_{mv} \right]. \end{aligned} \quad (36)$$

where the kernel functions $U_{mt,s/v}$, $U_{mc,s/v}$, $W_{mc,s}$, $V_{sd,s/v}$, $X_{sd,s/v}$, $W_{sd,s}$ are given by

$$U_{mt,s} = (\tilde{M}_a + \tilde{M}_b + 2\tilde{M}_c)(\tilde{T}_a + \tilde{T}_b + 2\tilde{T}_c)^*, \quad (37)$$

$$U_{mt,v} = (\tilde{M}_a - \tilde{M}_b)(\tilde{T}_a - \tilde{T}_b)^*, \quad (38)$$

$$U_{mc,s} = (\tilde{M}_a + \tilde{M}_b + 2\tilde{M}_c)(\tilde{C}_a - \tilde{C}_b)^*, \quad (39)$$

$$W_{mc,s} = 2(\tilde{M}_a + \tilde{M}_b + 2\tilde{M}_c)\tilde{C}_c^*, \quad (40)$$

$$U_{mc,v} = (\tilde{M}_a - \tilde{M}_b)(\tilde{C}_a + \tilde{C}_b + \tilde{C}_d)^*, \quad (41)$$

$$V_{sd,s} = (\tilde{M}_a + \tilde{M}_b + 2\tilde{M}_c) (\tilde{Q}_a + \tilde{Q}_b + 8\tilde{Q}_c)^*, \quad (42)$$

$$W_{sd,s} = (\tilde{M}_a + \tilde{M}_b + 2\tilde{M}_c) (\tilde{Q}_a + \tilde{Q}_b + 2\tilde{Q}_d)^*, \quad (43)$$

$$X_{sd,s} = (\tilde{M}_a + \tilde{M}_b + 2\tilde{M}_c) (\tilde{Q}_a - \tilde{Q}_b)^*, \quad (44)$$

$$V_{sd,v} = (\tilde{M}_a - \tilde{M}_b) (\tilde{Q}_a - \tilde{Q}_b)^*, \quad (45)$$

$$X_{sd,v} = (\tilde{M}_a - \tilde{M}_b) (\tilde{Q}_a + \tilde{Q}_b)^*. \quad (46)$$

The superscript $[n]$ in Eqs. (34-36) represents the n th moment of the Legendre expansion of the kernel function. For instance,

$$U_{mt,s}^{[n]} = \frac{1}{2} \int_{-1}^1 U_{mt,s} P_n(\hat{p} \cdot \hat{q}) d(\hat{p} \cdot \hat{q}). \quad (47)$$

Relevant loop integrals

The three-point loop integral that involves the insertion of the charge or magnetic operator is given by

$$\begin{aligned} \mathcal{J}_0 = & \int \frac{d^4 l}{(2\pi)^4} iS(-B_d + l_0, \mathbf{l}) iS(-B_d + l_0 + \omega, \mathbf{l} + \mathbf{q}) \\ & \times iS(-l_0, \mathbf{l}) \\ = & -m_N^2 \int \frac{d^3 l}{(2\pi)^3} \frac{1}{(l^2 + \gamma^2) \left[(\mathbf{l} + \frac{\mathbf{q}}{2})^2 - p^2 - i\epsilon \right]} \\ = & -\frac{m_N^2}{2\pi q} \arctan \frac{q/2}{\gamma - ip}. \end{aligned} \quad (48)$$

The loop integral $\mathcal{J}_{c,0}$ results from the convection current operator inserted in the diagrams shown Fig. 1. It contributes to the LO part of the amplitude \tilde{C}_c and is evaluated as follows:

$$\begin{aligned} \mathcal{J}_{c,0} = & \int \frac{d^4 l}{(2\pi)^4} iS(-B_d + l_0, \mathbf{l}) iS(-B_d + l_0 + \omega, \mathbf{l} + \mathbf{q}) \\ & iS(-l_0, \mathbf{l}) \frac{2\mathbf{l} + \mathbf{q}}{2m_N} \\ = & -m_N \int \frac{d^3 l}{(2\pi)^3} \frac{\mathbf{l} + \frac{\mathbf{q}}{2}}{(l^2 + \gamma^2) \left[(\mathbf{l} + \frac{\mathbf{q}}{2})^2 - p^2 - i\epsilon \right]} \\ = & \frac{\mathbf{q}}{q^2} \left[\frac{m_N}{4\pi} (\gamma + ip) + \omega \mathcal{J}_0 \right], \end{aligned} \quad (49)$$

To evaluate the NLO component of \tilde{C}_c , we need the loop integral with the convection current inserted in Fig. 1. This integral is divided into two parts: $\mathcal{J}_{c,2} = \mathcal{J}_{c,2}^{(0)} + \mathcal{J}_{c,2}^{(1)}$, where $\mathcal{J}_{c,2}^{(0)}$ includes the LO final-state interaction, and gives a zero contribution.

$$\begin{aligned} \mathcal{J}_{c,2}^{(0)} &= \frac{C_{2,-2}}{2} \mathcal{I}_0(-B_d) \int \frac{d^4 l}{(2\pi)^4} iS(-B_d + l_0 + \omega, \mathbf{l} + \mathbf{q}) \\ &\quad iS(-l_0, -\mathbf{l}) iS(-B_d + l_0, \mathbf{l}) \frac{2\mathbf{l} + \mathbf{q}}{2m_N} (l^2 + \gamma^2) \\ &= -\frac{C_{2,-2}}{2} \mathcal{I}_0(-B_d) m_N \int \frac{d^3 l}{(2\pi)^3} \frac{\mathbf{l} + \frac{\mathbf{q}}{2}}{(\mathbf{l} + \frac{\mathbf{q}}{2})^2 - p^2 - i\epsilon} \\ &= 0. \end{aligned} \quad (50)$$

$\mathcal{J}_{c,2}^{(1)}$ involves the NLO final-state interaction, and is given by

$$\begin{aligned} \mathcal{J}_{c,2}^{(1)} &= \int \frac{d^4 l}{(2\pi)^4} iS(-B_d + l_0, \mathbf{l}) iS(-B_d + l_0 + \omega, \mathbf{l} + \mathbf{q}) \\ &\quad iS(-l_0, -\mathbf{l}) \frac{\mathcal{A}_t^{(1)}(\mathbf{l} + \frac{\mathbf{q}}{2}, \mathbf{p}, E_f)}{\mathcal{A}_t^{(0)}(E_f)} \frac{2\mathbf{l} + \mathbf{q}}{2m_N} \\ &= \frac{\rho}{2} \left[(\gamma - ip) \mathcal{J}_{c,0} - \frac{m_N}{2(\gamma - \mu)} \int \frac{d^3 l}{(2\pi)^3} \frac{\mathbf{l} + \frac{\mathbf{q}}{2}}{l^2 + \gamma^2} \right] \\ &= \frac{\rho \omega \mathbf{q}}{2q^2} \left[\frac{m_N^2}{4\pi} + (\gamma - ip) \mathcal{J}_0 \right]. \end{aligned} \quad (51)$$

The transition amplitude that involves the S-D mixing operator, shown in Fig. 3, contains two three-point loop integrals.

$$\begin{aligned} \mathcal{J}_{Q1} &= \int \frac{d^4 l}{(2\pi)^4} iS(l_0 + \omega, \mathbf{l} + \mathbf{q}) iS(-l_0 - B_d, -\mathbf{l}) \\ &\quad iS(l_0, \mathbf{l}) \left[\left(l_i + \frac{q_i}{2} \right) \left(l_j + \frac{q_j}{2} \right) - \frac{1}{3} \left(\mathbf{l} + \frac{\mathbf{q}}{2} \right)^2 \delta_{ij} \right] \\ &= -m_N^2 \int \frac{d^3 l}{(2\pi)^3} \frac{l_i l_j - \frac{1}{3} l^2 \delta_{ij}}{\left[\left(\mathbf{l} - \frac{\mathbf{q}}{2} \right)^2 + \gamma^2 \right] [l^2 - p^2 - i\epsilon]} \\ &= \bar{J}_{Q1} \left(q_i q_j - \frac{1}{3} q^2 \delta_{ij} \right) / q^2, \end{aligned} \quad (52)$$

$$\begin{aligned} \mathcal{J}_{Q2} &= \int \frac{d^4 l}{(2\pi)^4} iS(l_0 + \omega, \mathbf{l} + \mathbf{q}) iS(-l_0 - B_d, -\mathbf{l}) \\ &\quad \times iS(l_0, \mathbf{l}) \left[l_i l_j - \frac{1}{3} l^2 \delta_{ij} \right], \\ &= \bar{J}_{Q2} \left(q_i q_j - \frac{1}{3} q^2 \delta_{ij} \right) / q^2, \end{aligned} \quad (53)$$

where the amplitudes \bar{J}_{Q1} and \bar{J}_{Q2} are given as

$$\begin{aligned} \bar{J}_{Q1} &= \frac{m_N^2}{16\pi q^3} \left\{ q \left[q^2 \gamma + 6m_N \omega (\gamma + ip) \right] \right. \\ &\quad \left. + 4 \left[q^2 p^2 - 3m_N^2 \omega^2 \right] \arctan \frac{q/2}{\gamma - ip} \right\}, \end{aligned} \quad (54)$$

$$\begin{aligned} \bar{J}_{Q2} &= -\frac{m_N^2}{16\pi q^3} \left\{ q \left[iq^2 p + 6m_N \Omega (\gamma + ip) \right] \right. \\ &\quad \left. + 4 \left[q^2 \gamma^2 + 3m_N^2 \Omega^2 \right] \arctan \frac{q/2}{\gamma - ip} \right\}, \end{aligned} \quad (55)$$

with $\Omega = (-p^2 - \gamma^2 + q^2/4)/m_N$. Their combination yields

$$\begin{aligned} \bar{J}_Q &= \bar{J}_{Q1} + \bar{J}_{Q2} \\ &= \frac{m_N^2}{32\pi q^3} \left\{ 2q(\gamma - ip) \left[q^2 + 12(\gamma + ip)^2 \right] - [48(p^2 + \gamma^2)^2 \right. \\ &\quad \left. + 8q^2(\gamma^2 - p^2) + 3q^4 \right] \arctan \frac{q/2}{\gamma - ip} \right\}. \end{aligned} \quad (56)$$

Trace algebra summation

The np spin-isospin projection operators, denoted as Π_α , satisfy the trace identity $\text{Tr} \left[\Pi_\alpha \Pi_\beta^\dagger \right] = \frac{1}{2} \delta_{\alpha\beta}$ and $\text{Tr} \left[\Pi_\alpha \tau_3 \Pi_\beta^\dagger \right] = 0$, with $\alpha, \beta = 0, \pm$. These projection operators anti-commute with the isospin operator τ_3 .

The nuclear response functions are connected to the transition matrices by employing the trace summation:

$$\text{Tr} \left[\Pi_+ \boldsymbol{\sigma} \Pi_+^\dagger \right] = \text{Tr} \left[\boldsymbol{\sigma}^T \Pi_+ \Pi_+^\dagger \right] = (0, 0, \frac{1}{2}), \quad (57)$$

$$\text{Tr} \left[\Pi_+ \boldsymbol{\sigma} \tau_3 \Pi_+^\dagger \right] = \text{Tr} \left[\tau_3 \boldsymbol{\sigma}^T \Pi_+ \Pi_+^\dagger \right] = (0, 0, 0), \quad (58)$$

$$\text{Tr} \left[\Pi_+ P_i^\dagger \right]^* \text{Tr} \left[\Pi_+ \boldsymbol{\sigma} P_j^\dagger \right] = \mathbf{b}_{ij}, \quad (59)$$

where \mathbf{b}_{ij} equals

$$\mathbf{b}_{ij} = \frac{1}{8} \left\{ \begin{pmatrix} 0 & 0 & -1 \\ 0 & 0 & -i \\ 0 & 0 & 0 \end{pmatrix}_{ij}, \begin{pmatrix} 0 & 0 & i \\ 0 & 0 & -1 \\ 0 & 0 & 0 \end{pmatrix}_{ij}, \begin{pmatrix} 1 & -i & 0 \\ i & 1 & 0 \\ 0 & 0 & 0 \end{pmatrix}_{ij} \right\}. \quad (60)$$

-
- [1] J.-W. Chen, G. Rupak, and M. J. Savage, *Nucl. Phys. A* **653**, 386 (1999).
 - [2] S. B. Emmons, C. Ji, and L. Platter, *J. Phys. G* **48**, 035101 (2021).
 - [3] J.-W. Chen, G. Rupak, and M. J. Savage, *Phys. Lett. B* **464**, 1 (1999).
 - [4] S.-i. Ando and C. H. Hyun, *Phys. Rev. C* **72**, 014008 (2005).